Full-scale flying shape measurement of offwind sails with photogrammetry

Julien Deparday[♡], Patrick Bot[♡], Frederic Hauville[♡], Benoit Augier[♡], Marc Rabaud[♣]

[♡] *Naval Academy Research Institute - IRENAV CC600, 29240 BREST Cedex 9, France*

[♣] *Laboratoire FAST, Univ. Paris-Sud, CNRS, Université Paris-Saclay, F-91405, Orsay, France*

Abstract

Yacht downwind sails are complex to study due to their non-developable 3D shape with highly cambered sections and massively detached flow around a thin and very flexible membrane. Advanced numerical simulations can now simulate this strong fluid-structure interaction problem; however such simulations need experimental validation. At full-scale, measuring the spinnaker shape in real sailing conditions (flying shape) is also valuable for sail designers as they would benefit a feedback for their designs. Nonetheless it remains complex to measure spinnaker flying shapes partly because of their inherent instability, like flapping of the luff. This work presents a full-scale experimental investigation of spinnaker flying shapes with simultaneous measurement of the aerodynamic loads on the three sail corners, as well as navigation and wind data. The developed experimental set-up and photogrammetric method to acquire the flying shape of the spinnaker are presented. Results are analysed for four different apparent wind angles and measured flying shapes are

Email address: patrick.bot@ecole-navale.fr (Patrick Bot[♡])

compared with the sail shape defined by the sail designer (design shape). The photogrammetric measurement produces the full 3D flying shape with a satisfactory accuracy determined in this paper. This new system enables time-resolved measurement of flying shapes and thus flapping of spinnakers to be investigated, which is valuable for performance optimisation of sailing yachts. On top of sailing yacht applications, the method might be useful in any application where a non-developable 3D shape is to be determined, and particularly when it results from the Fluid Structure Interaction of a flexible structure with a complex flow.

Keywords:
Fluid Structure Interaction, Full-Scale experiment, Photogrammetry, Yacht Sails, Soft Membrane

---

1. Introduction

Performances achieved by recent racing yachts demonstrate the massive improvements made in yacht design, materials and fabrication. In hull design, rigging design or sail design, more and more detailed research and development are used to be competitive. Understanding the physics and thus the behaviour of racing yachts have been enabled by many experimental studies combined with advanced computational resources reached nowadays. In sail design, from traditional and empirical manufacture, best sail designers now use high technology materials and important research and development tools (Braun and Imas (2008); Ranzenbach et al. (2013)).

The need of acquiring flying shapes, stressed by Ranzenbach and Kleene

(2002), has also been an important development. The shape while sailing -also called flying shape- gives valuable information for validation of numerical simulations, for comparison of shapes at different apparent wind angles (AWA) and with the design shape -drawn by the sailmaker-.

On the water, sail shapes and performance measurements have already been carried out by the sail dynamometer boat Fujin (Masuyama (2014)). Another sail dynamometer boat called DYNA had a flying shape measurement system described in Clauss et al. (2005). However those sail dynamometer boats mainly focused their experiments in upwind situations. A sail analyser method called Visual Sail Position And Rig Shape (VSPARS) is developed by the Yacht Research Unit at the University of Auckland (Le Pelley and Modral (2008)). North Sails has also developed their own tool called Advanced Sail Analyser (ASA). However, all those systems have a strong hypothesis for accurate measurements: the stripes painted or glued on the sail, are supposed to remain in a horizontal plane, which is not always the case for flying sails on a large range of apparent wind angles.

For downwind conditions, the physics is by far more complex than in upwind conditions due to strongly coupled fluid-structure interaction between a highly curved flow and light sail cloth. Compared to upwind conditions, soft and flexible offwind sails have an inherent unsteadiness even in conditions considered "stable" (with no gust, no wind shift, on flat water and fixed trimming). This phenomenon can be spotted as a flapping at the leading edge, also called luffing. Some numerical simulations can now model the dynamic behaviour of downwind sails (Durand et al. (2014); Lombardi et al. (2012)). However those simulations need validation from experiments to be

confidently used in sail design optimisation. Different tools have been used to measure flying shapes of downwind sails during wind tunnel experiments at smaller scale: Coordinate Measuring Machine (Ranzenbach and Kleene (2002)), Photogrammetry measurement (Fossati (2009)) with custom built Infrared cameras and Renzsch and Graf (2013). Nevertheless for wind tunnel experiments, some rules of similitude are violated. Not only is there a too small Reynolds number (about 4.10^6 for full scale testing and 4.10^5 for a 1/10th model) but also a different ratio of fabric weight to wind pressure is encountered as well as a different ratio of membrane stress to wind pressure. Thus full-scale experiments would complete the validation. At full scale, we have previously investigated pressure evolution during luffing (Deparday et al. (2014); Motta et al. (2015)).

To measure the shape of a thin flexible surface several methods have been developed. Photogrammetry and videogrammetry using dot projection has been used on solar sails by NASA (Pappa et al. (2003)). Stereophotogrammetry permits to measure deformations of a flexible wing in a wind tunnel (Pitcher et al. (2009)). But only small displacements and wrinkles are measured. Thin flexible surfaces like a spinnaker can have large displacements, in an order of magnitude of 1 to 5 m. Techniques to measure the displacement of a surface exist e.g. the optical profilometric technique measuring free-surface deformations using fringe pattern projection (Cobelli et al. (2009)). However for those methods a controlled environment is required. Salzmann and Fua (2011) developed a model using a deforming mesh corresponding to the size of the object and only one camera. Nevertheless given the large

area of the spinnaker, it is not guaranteed the whole sail is in the field of view of only one camera fixed on the deck of the sailing yacht. Those last years laser measuring tools like LIDAR (LIght Detection and RAnging) have been improved and can be used to measure flexible sails. However because of the large time necessary to scan the whole sail, dynamic measurement might be difficult to obtain. The sampling rate and the accuracy can significantly decrease with moderate cost laser measuring tools. Considerable work needs to be achieved to obtain accurate data, like the custom patented system developed by Fossati et al. (2015b) using a "Time-Of-Flight" radar to detect flying shapes. It will be used on their sail dynamometer boat (Fossati et al. (2015a)).

To obtain a 3D-shape of a flying spinnaker, we decided to use photogrammetry process. In Mausolf et al. (2011), full-scale flying shapes of spinnakers were captured using a photogrammetry process with 4 cameras placed on motorboats all around the sailing yacht, which requires manpower. In addition with independent and spaced cameras, synchronization is hard to obtain with all the cameras and with the other time-resolved data. Moreover they are on moving spots relative to the sailing yacht, which is not convenient for time-resolved flying shape measurements. Furthermore rigid-inflatable boats create waves and can hamper experiments.

Moreover, those last couple of years have witnessed an increase in the quality of cameras and a considerable cost reduction. High resolution cameras are now more affordable for experiments. If the positions of cameras are unknown, a minimum of 3 photographs is required for photogrammetry measurement. However for redundancy and better accuracy, more photographs

are needed. We decided to use six High Definition cameras with wide field of views to see the sail from different angles. They were fixed on the sailing yacht on the deck. The actual locations of the cameras do not need to be known for flying shape reconstruction. At last, placing cameras on deck avoid occlusion issues with the mainsail.

In this paper, we present a full scale testing where aerodynamic loads and flying shape are simultaneously measured. Those data are time-resolved to be used for validation of numerical models and to better assess unsteady aerodynamics of offwind sails taking into account luffing for example. We present here the experimental setup and the first steady results for four different apparent wind angles (AWA): 64° , 96° , 124° and 141° . The accuracy of the photogrammetric flying shape acquisition system is discussed. Then flying shapes are compared between each other. We present a new method for comparison using the volume distribution. It is defined as the projection of depth of the sail onto the plane created by the 3 corners of the spinnaker (head, tack and clew). The last section deals with the comparison between the design shape and the flying shapes.

2. Experimental Setup

While sailing downwind, we simultaneously measured the flying shape of the spinnaker as well as the loads on the rigging and on the corners of the spinnaker, the motion of the boat and the navigation parameters including the wind. We used a J/80 class yacht, an 8 meter one-design cruiser racer. A

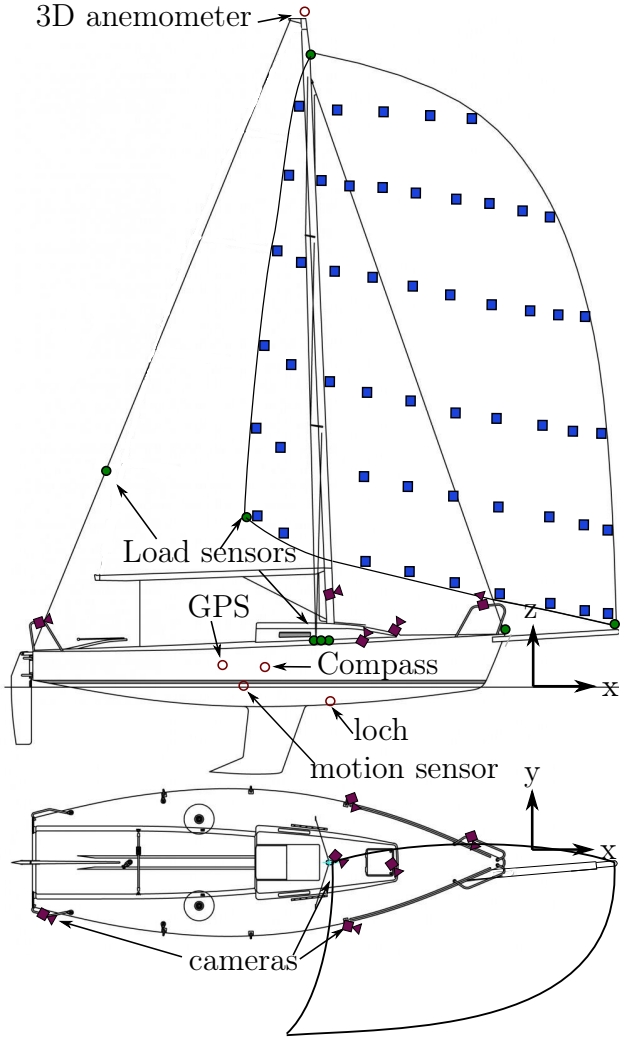

Figure 1: General arrangement of the experimental set-up on the J/80. 11 load sensors (green discs), 6 cameras (purple objects), and wind and boat sensors (red circles). Sail markers (blue squares).

tri-radial spinnaker with a surface of 65 m^2 with a 12 meter long rounded luff was hoisted. Figure 1 presents the general layout of the experimental setup. A repeatable procedure was applied during experiments. All data were

recorded "on the flow", at their own rate using a dedicated programmable automation controller. A post-processing routine is used to obtain synchronous data for easier analysis. To ease and speed up comparison with numerical simulations, for the experiments described in this paper, the mainsail was not hoisted. Nevertheless with the present system, the flying shape of the spinnaker can be acquired with the mainsail up.

2.1. Loads

Aerodynamic loads are measured using strain gauges. Forestay, shrouds, backstay are equipped with dedicated instrumented turnbuckles and shackles. This measurement system for standing rigging is more described in Augier et al. (2012). The measurement error is less than 2% of the measurement range of 5000 N (10 000 N for the shrouds and forestay). The sampling frequency is 25 Hz. The sensors on the standing rigging are wired to the programmable automation controller which has a dedicated acquisition system for strain gauges. The three corners of the spinnaker (head, tack and clew) are fitted with dedicated strain gauges communicating with the controller via a wireless low consumption ZigBee protocol. The error of measurement and the sampling frequency are identical to those for standing rigging (i.e. 2% of the measurement range and 25 Hz).

2.2. Boat data

Speed and course over ground from a GPS, speed and course above water from a speedo and a compass are gathered by a NKE interface. All

those data are also sent at various sampling frequencies from 1 to 5 Hz, to the programmable automation controller using serial communication with NMEA-type sentences.

At the mast head a 3D ultrasonic anemometer records the wind velocity and the 3D wind direction at 10 Hz.

2.3. Flying Shape acquisition

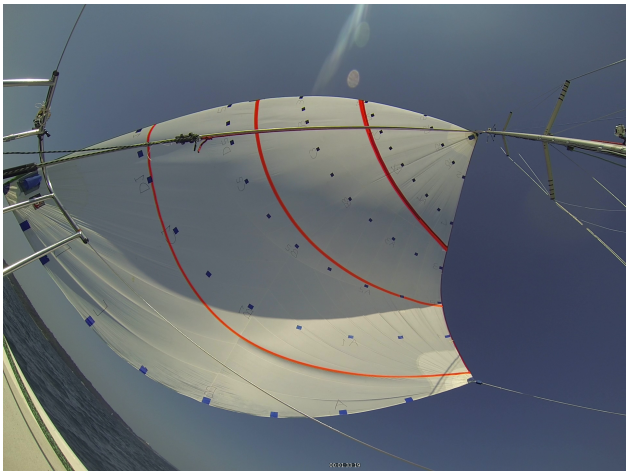

Figure 2: Photograph of the spinnaker used with squared targets distributed on the sail. View from one camera centred on the deck.

To obtain a 3D-shape of a flying spinnaker, we used a photogrammetry process.

Before the experiments, the sail is fitted with 51 dark blue markers $100 \times 100\,\mathrm{mm}^2$ wide at discrete points. Figure 2 shows this layout. Six rows of dark blue targets are stuck on the sail cloth. Those rows divide the luff and

leech in 6 equidistant sections. On those rows, targets are evenly distributed from the leading edge to the trailing edge. An additional target is placed in the first 10% of the row in order to acquire a more accurate leading edge curve. The three corners (head, tack and clew) are also marked.

Before the experiments, a thorough calibration of the cameras is applied. The focal length, principal points and distortion due to the fish-eye lens are determined for each camera in their experimental configurations with their housings. With these known parameters, it is possible to determine the position of cameras during post-processing, using many points detected on different images.

From previous tries, 6 outdoor purpose cameras are placed to observe the most of the spinnaker for various apparent wind angles (from 70° to 140°). Three cameras is the minimum required. However, the more the better for redundancy and to increase accuracy. Nevertheless, too many cameras close to each other do not enhance the accuracy, since tight angles between cameras increase the error in depth. Using 6 cameras is a good compromise for such sail. They possess wide field of view of about 140°. Two of the cameras are GoPro Hero 3 Black with a resolution of 2560x1440 (3.7Mpixels). The others (3 GoPro Hero 2 and 1 GoPro Hero 3 Silver) have a resolution of 1920x1080 (2.07Mpixels). The frame rate is 25 Hz. The videos are stored locally in micro-SD cards. The cameras are positioned on the sailing yacht at vantage points, on the pushpit, pulpit, deck-hull connection (starboard and portside), on the foredeck and on the mast -1.5 m up from the deck-

(see Fig. 1). However the actual locations of the cameras do not need to be known for flying shape reconstruction. The cameras are switched on simultaneously. The post-synchronisation of every video is possible thanks to a laser aiming the sail every 10 seconds during 0.1 s. This laser signal is also recorded with all the other time-resolved data.

During the experiments, movies are taken from those 6 different positions on the sailing yacht.
An algorithm of photogrammetry from the software PhotoModeler developed by Eos Systems Inc. (2015) is used. From each image the position of a target is known in a 2D space. The third coordinate, the depth is computed where the perspective rays of the same target from different images are intersected (see Fig. 3). Those targets create a 3D point cloud which needs to be scaled and rotated. From different precise measured distances (i.e. between spreaders, from tack point to mast foot, etc.), those 3D targets are positioned in a reference frame with x along the longitudinal axis of the boat, y to portside and z pointing upwards.
Finally, these points are lofted to create spline curves. From those curves, a Non Uniform Rational B-Splines (NURBS) surface is created to represent the 3D-shape of a flying spinnaker.

2.4. Procedure

Experiments have been carried out on a J/80 yacht, in the bay of Brest, offshore Ecole Navale in July 2014. Wind direction was North East, wind average speed 12 kn (6.2 m/s) with gusts at 15 kn (7.7 m/s), flat water (wave

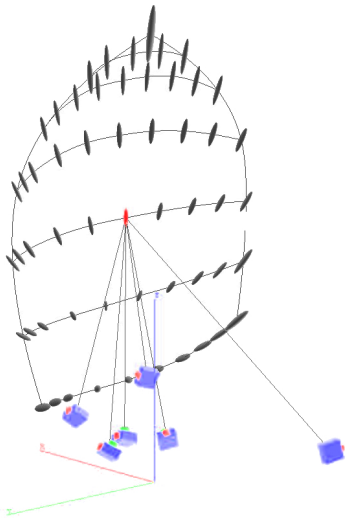

Figure 3: Perspective rays (black lines) from cameras (in blue) to one point on the spinnaker (in red). Every bulb represents the confidence region for every point. (Bulbs are scaled up 20 times).

height $\approx 0.1\,\mathrm{m}$).

A detailed procedure helps for correct measurements to be repeatable and usable. Every test is repeated several times for every apparent wind angle (AWA).

- Sail at a constant given AWA.
- Spinnaker is slightly overtrimmed (i.e. no flapping of the leading edge) for one minute minimum.
- During the post-processing routine, 20 second long periods were labelled "stable" when the standard deviation of the AWA was below 6° and the standard deviation of the apparent wind speed (AWS) was

below 10% of the average.

- Best "stable periods" –with lowest standard deviations on wind data- were selected for each AWA. Their corresponding flying shapes are presented in this article.

3. Results

In this section, we will describe 4 different flying shapes at distinct apparent wind angles presented in Figure 4: 64°, 96°, 124° and 141°. For each apparent wind angle, the spinnaker is slightly overtrimmed (the luff does not flap). The flying shape is fairly constant during the 20 second "stable" period described before. Thus the flying shape of one timestamp has been chosen to be representative of the average flying shape.

3.1. Accuracy of the flying shape acquisition

From those flying shapes, the precision and accuracy of the flying shape acquisition are quantified.

3.1.1. Precision

Precision calculated by the photogrammetry process of PhotoModeler helps to quantify the error of our system. Calculating the positions of the cameras and points on the spinnaker is an iterative process. Thus the uncertainties on positions - the residuals - are analysed.
Table 1 shows the precision defined as one standard deviation based on the

Table 1: Standard deviation in mm based on the post-processing covariance matrix of the 3D object points. Three last columns decompose the average precision in the boat frame (X longitudinal, Y portside and Z upwards).

AWA	Average Precision (mm)	X Precision (mm)	Y Precision (mm)	Z Precision (mm)
64°	38	13	12	29
96°	30	12	10	24
124°	27	11	9	21
141°	21	9	7	16

post-processing covariance matrix of the 3D object points. The second column shows the average precision of all points computed for each apparent wind angle. The three next columns are the decomposition of this average precision in the boat frame. The precision is displayed and scaled up 20 times in Figure 3 as the "confidence region" for every point.

The precision is in average better than 40 mm, 0.3% of the luff length. Precision in Z axis (upwards) is worse than in other axes due to similar height positions of camera -on the deck- . At the head of the spinnaker, about 10 m away from the cameras, the angles between the perspective rays from cameras are sharp and the markers at the top of the spinnaker have lower resolution. This is why in Figure 3 points near the spinnaker head have a larger confidence region. Only 3% of all the computed points have an error larger than 100 mm.

3.1.2. Accuracy

Comparing measured lengths on ground with no tension applied in the sail cloth and from the computed flying shape is a way to evaluate the accuracy of our system. Table 2 shows the lengths of the luff, leech and foot

Table 2: Comparison of lengths measured on ground with a measuring tape and measured with the flying shape acquisition system for different apparent wind angles. Percentages are the ratio between difference of measurements and ground measured lengths.

AWA	foot (m)	luff (m)	leech (m)	SA (m^2)
ground	7	12	9.6	
64°	7.2 3.40%	12.3 2.20%	9.7 1.80%	66.5
96°	7.1 1.30%	12.2 1.60%	9.7 1.10%	65.1
124°	7.2 3.40%	12.4 3.20%	9.8 4.00%	68.7
141°	7.2 2.80%	12.3 2.70%	9.8 2.30%	67.4

for the four different apparent wind angles calculated by our photogrammetry acquisition system. The errors are less than 4% for all apparent wind angles. Moreover all dimensions displayed in Table 2 are overestimated. To cancel out this error, ground measured lengths should be increased by 2.3%, which is consistent knowing the possible measurement errors with a ruler and the elasticity of the sail. This is indeed in the order of magnitude of elongation of a spinnaker cloth for the loads measured during our experiments (around 400 N). The Sail Area is not compared to a reference value due to the difficulty to measure accurately by hand a non-developable surface. The maximum difference between the measured sails is 3.6 m^2, which corresponds to 5% of the average measured area.

3.2. Presentation of the flying shapes

Figure 4 presents 4 flying shapes from AWA 64° to 141° with the corresponding measured heel. Figure 4c displays the bird's eye view above the mast perpendicular to the X-Y plane of the boat. The arrow represents the apparent wind direction measured at the top of the mast. At 64°, the clew point is aft the mast and the whole luff is on the leeward side of the boat. The luff is slightly folded as it is common at tight apparent wind angles. When the apparent wind angle is increased, the clew point goes further forward and upward. Between AWA 64° and 141°, the clew point position is 2.3 m more forward and 1.4 m higher and goes only 0.5 m more to the leeward side. Thus the clew point is closer to the "tack-head" line. Still, the same sail area is held by those 3 points while the area of the triangle head-tack-clew is smaller. Thus for deeper AWA, the spinnaker has a more rounded shape with the luff rotating to the windward side and with the leech more opened

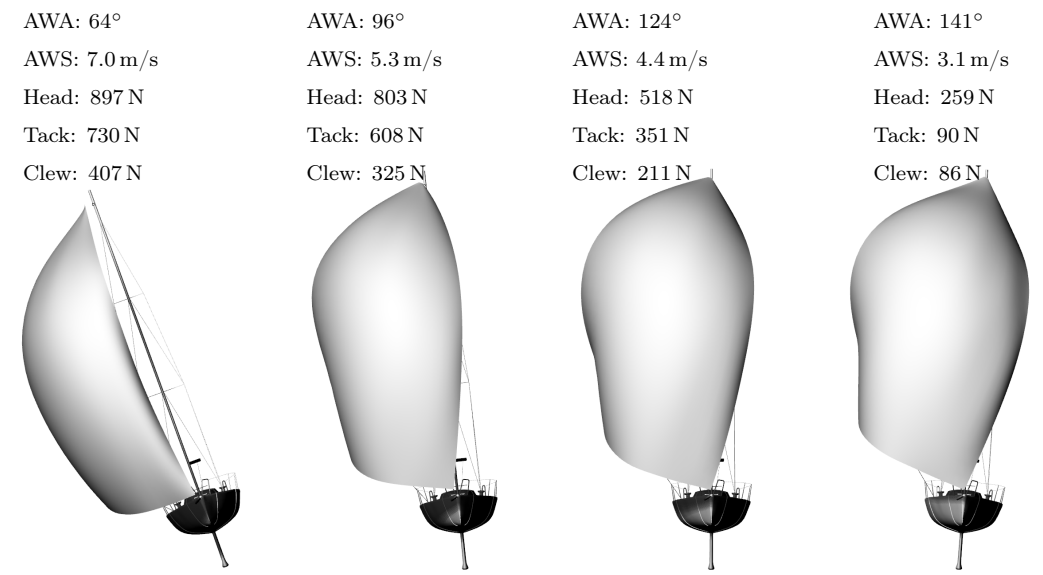

(a) View from front

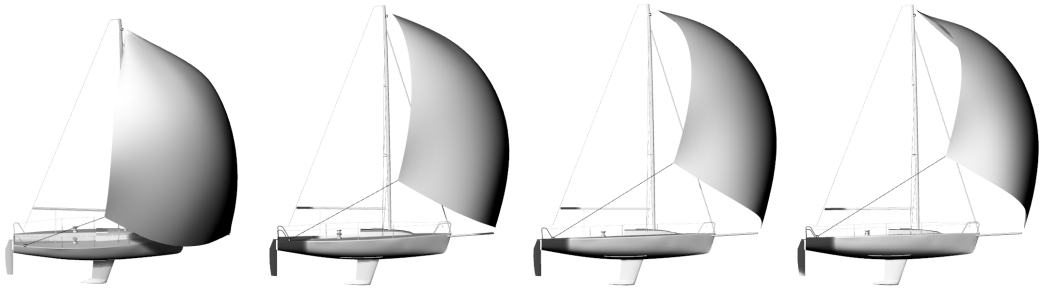

(b) View from starboard

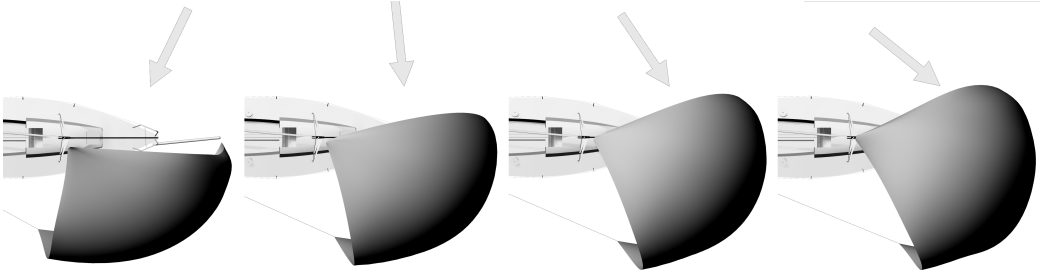

(c) Bird's eye view just above the mast head

Figure 4: 3D views of 4 flying shapes with corresponding loads at the head, tack and clew. From left to right AWA: 64° , 96°, 124°, 141°.

at 3/4 height.

Table 3: Main surface geometric parameters for 6 sections for two different apparent wind angles. The reference for percentages is the chord length. Twist is defined as the horizontal angle between the chord of a stripe and the chord of the foot. All data is measured by the photogrammetry process.

Section	curve	**AWA** 64°				**AWA** 124°			
	length (m)	chord (m)	max camber	draft	twist	chord (m)	max camber	draft	twist
foot	7.19	6.58	20%	49%	-	5.93	31%	41%	-
1/6	7.66	6.51	25%	44%	12°	6.29	31%	46%	13°
2/6	7.78	6.31	27%	39%	21°	6.5	28%	46%	27°
3/6	6.96	5.8	26%	44%	32°	6.16	24%	48%	41°
4/6	5.04	4.53	18%	45%	33°	4.69	20%	49%	57°
5/6	2.54	2.33	15%	61%	35°	2.4	18%	67%	69°

Sail designers commonly use sections at different heights to create design shape of spinnaker. Leech and luff are divided into equidistant segments. Each division on the luff linked to a division on the leech defines a section at a specific height. They are convenient to design a sail or compare the flying shape evolution.

For two significant apparent wind angles, 64° and 124°, Table 3 displays some typical surface geometric parameters for 6 sections defining the spinnaker. At AWA 64° the maximum of camber is found at 1/3 of the spinnaker height, while at AWA 124° the maximum of camber is found near the foot. The spinnaker bottom is flatter at AWA 64° than at AWA 124° with a lower camber and longer chord for a similar draft position. For AWA 124°, the spinnaker is more opened at the top producing longer chord lengths than at AWA 64°. For larger apparent wind angle, the clew position is more forward and higher

allowing a more twisted shape. Table 3 indicates there is a small twist in the lower part of the spinnaker for the AWA 64°, while at AWA 124° the twist increases constantly from bottom to top of the sail.
However, the stripes are not always contained in a plane parallel to the flow. They can be curved, and have different heights at the luff and leech points. Unlike upwind sails, spinnakers are far from 2D-extruded shapes. Downwind sails are 3D objects. Therefore, those geometric sections might not be the most convenient way to quantify the 3D geometry of a spinnaker.

Figure 5 presents the shape of the spinnaker in a different way. It shows the "3D camber", the depth of the sail projected onto the plane created by the 3 corners of the spinnaker. The "H" point is the head of the spinnaker fixed on the mast and "T" is the tack point fixed on the bowsprit of the boat. Assuming those points fixed, with this representation the position of clew "C" is defined with the angles of the triangle HTC and the volume distribution of the spinnaker is displayed. This representation could facilitate the comparison between shapes.
The cross marker showing the location of the maximum of "3D camber" is located slightly above and forward the centroid of the triangle "Head-Tack-Clew" (HTC). At AWA 64°, the volume distribution is mainly homogeneous and circular. When the apparent wind angle is increased, the “bulb of camber” tends to have a more elongated and bended shape similar to a bean shape. Furthermore, for deeper AWA, the maximum of depth goes slightly aft. At AWA 141°, it is located at the middle of the Head median. Finally when the AWA is increased, the projected area decreases a bit while the vol-

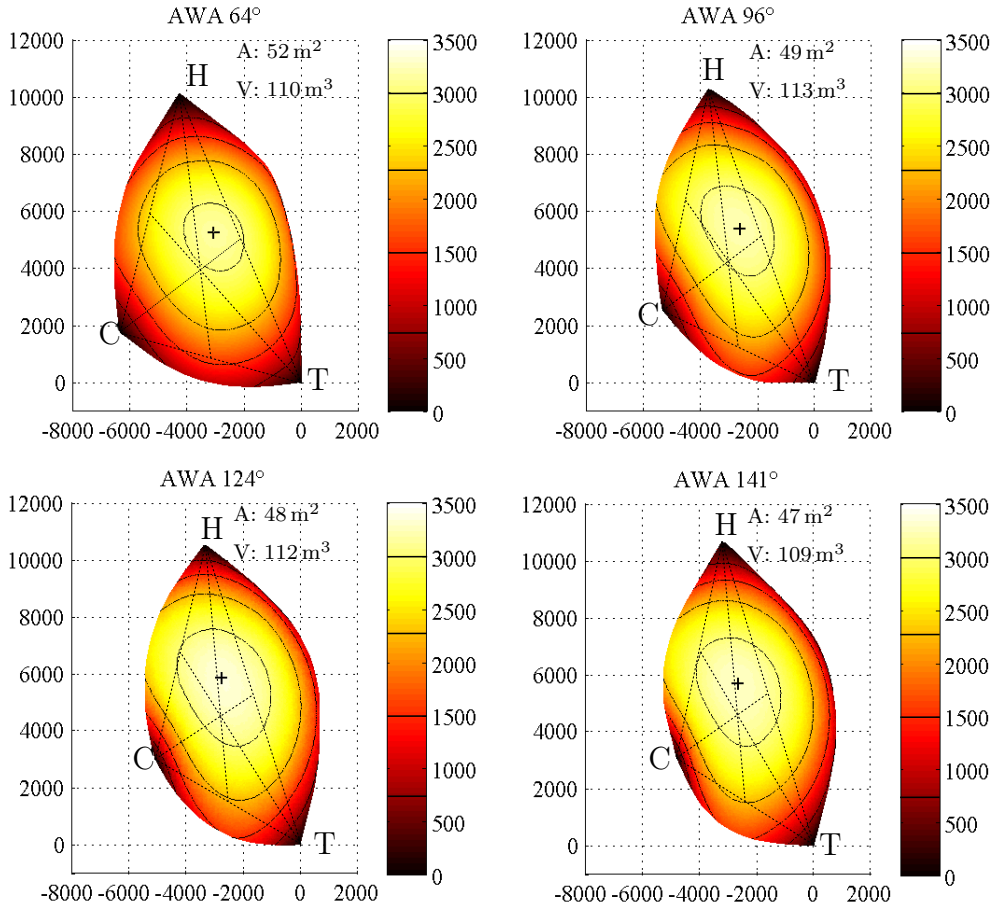

Figure 5: Depth of the spinnaker in mm projected onto the plane created by the 3 corners head (H)-tack (T)-clew (C) for different apparent wind angles. Black lines on the spinnaker represent isoheights. The cross marker represents the maximum depth location. For each AWA, the projected area (A) of the spinnaker onto the plane and the volume (V) between the spinnaker and the plane are given.

ume between the spinnaker and the HTC plane remains constant.

3.3. Comparison of the flying shapes with the design shape

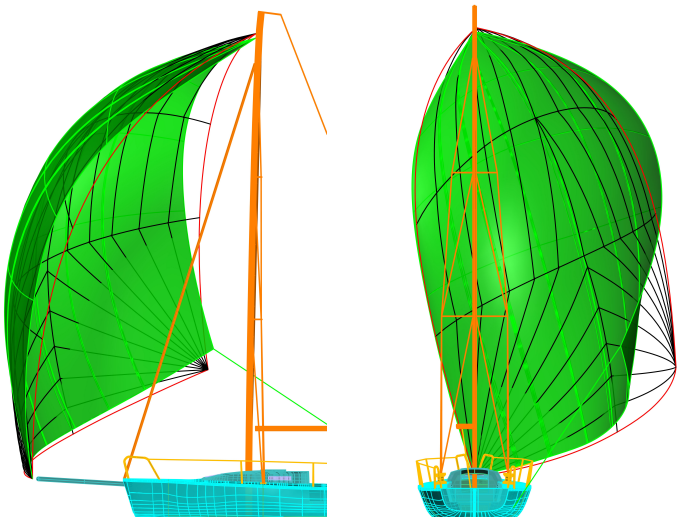

Figure 6: Comparison of design shape (in black lines and edges in red) and measured flying shape for AWA 124° (in green).

Figure 6 shows two distinctive shapes, the design shape of the spinnaker used during those experiments (in black lines and red edges) and the measured flying shape for AWA 124° (the green surface). The design shape is a generic shape. No specific trim or apparent wind angle is assumed during the design phase of the sail. The flying shape for AWA 124° was chosen because it corresponds to the best angle course downwind (best Velocity Made Good for a J/80 is around 120° in 12-16 knot wind). Compared with the flying shape, the design shape has less volume at half height of the sail with less rounded edges. At full scale, the leech is more curved, more opened at 3/4 height and closed at bottom due to the only control we have with the clew point. The design shape clearly diverges from the actual flying shape for best angle course downwind.

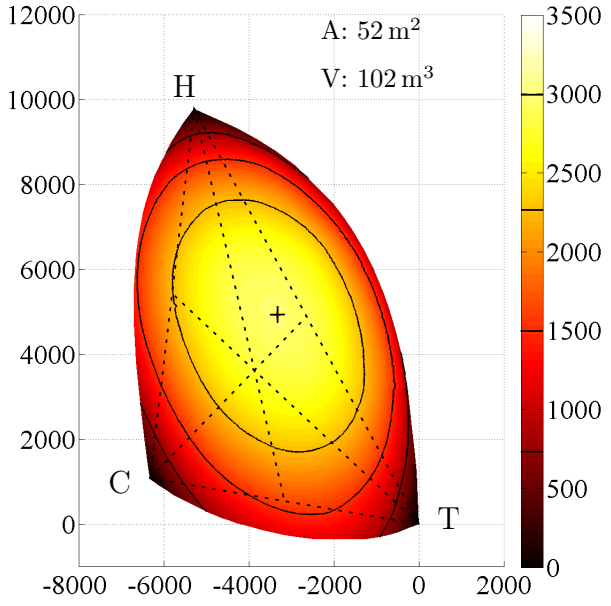

Figure 7: Depth of the design shape of the spinnaker in mm when projected onto the plane created by the 3 corners head-tack-clew. The projected area of the spinnaker onto the plane is A=52 m^2 and the volume between the spinnaker and the plane is V=102 m^2.

Figure 7 presents the design shape using the "3D camber" representation described before. It is compared with the "3D cambers" of the different flying shapes presented in figure 5.

The design shape is closer to the flying shape at AWA 64°. The clew positions are similar. With the points "T" and "H" fixed, the "head-tack-clew" triangle defines the position of the clew point. The clew angle for the design shape is 93° (90° for AWA 64°) and the tack angle is 52° (52° for AWA 64°). Moreover the projected area for the design shape is equal to the projected

area for AWA 64° (A=52 m^2).

However, not only is an apparent wind angle of 64° an extreme sailing navigation for this type of spinnaker, but also the design shape does not really correspond to any flying shapes presented in Figure 5. The "bulb of camber" is clearly elliptic, neither circular nor has a “bean shape”. The maximum of camber is slightly less than 3 m while the maximum camber on flying shapes is 3.3 m at AWA 124° and 3.1 m for AWA 64°. Moreover, between the design shape and the flying shape for AWA 64°, the volume between the spinnaker and the HTC plane is different (102 m^3 compared with 110 m^3), even though the positions of the 3 spinnaker points (head, tack and clew) and the projected area are identical. Thus the difference between the design and the flying shapes is not only due to a difference of trim but also results from the fluid-structure interaction between the wind and the sail.

The "3D camber" method underlines the discrepancies in terms of volume and projected surface for the different flying shapes, determining parameters in the design process. Acquiring real flying shapes would then help to improve the design of spinnakers.

4. Conclusion

An experimental set-up has been developed on a J/80 class sailing yacht to record time-resolved data of flying shapes, aerodynamic forces of the spinnaker and on the standing rigging, as well as boat motion and wind data. A new on-board system using a photogrammetry process is developed to capture the flying shape of the spinnaker with or without the mainsail hoisted.

Results of this process give reliable and sufficiently accurate data to compare flying shapes for different apparent wind angles with the design shape and thus would help sail designers and competitors.

The first static flying shapes have been captured during navigation and validated. The use of sections to define the shape of the sail surface is common but might not be the optimal solution for downwind sails because of the large curvatures and deformations. Displaying the volume distribution, the depth of the sail projected onto the plane created by the 3 corners of the spinnaker might be another good tool to compare shapes.

However the main purpose of this acquisition system is the possibility to acquire the inherent unsteadiness of offwind sails by resolving dynamic flying shapes. Analysing the evolution of shapes with loads and boat data during flapping and easing is possible and will be a significant benchmark for validation of unsteady Fluid Structure Interaction numerical simulations.

The method proved to be efficient to determine the real spinnaker flying shape resulting from the design shape to which the sail is made and the Fluid Structure Interaction with the sheered and twisted apparent wind flow. The new information provided will be very helpful to improve performances of sailing yachts. Moreover, the method can be used in any other application that needs to measure an unsteady 3D non-developable shape, particularly when it results from the Fluid Structure Interaction of a flexible structure with a complex flow.

Acknowledgements

The authors would like to thank DELTA Voiles for giving us the spinnaker and the design shape. They also would like to thank Eos Systems Inc. for their efficient help on PhotoModeler. The authors would also not forget to thank Ronan Floch from Incidences for the fruitful discussions they had together.

References

Augier, B., Bot, P., Hauville, F., Durand, M., 2012. Experimental validation of unsteady models for fluid structure interaction: Application to yacht sails and rigs. Journal of Wind Engineering and Industrial Aerodynamics 101, 53–66.
URL http://linkinghub.elsevier.com/retrieve/pii/S0167610511002352

Braun, J. B., Imas, L., 2008. High fidelity CFD simulations in racing yacht aerodynamic analysis. In: 3rd High Performance Yacht Design Conference. Auckland, pp. 168–175.

Clauss, G., Heisen, W., Berlin, D., 2005. CFD Analysis On The Flying Shape of Modern Yacht Sails. In: Proceedings of the 12th It. Congress of the International Maritime Association of the Mediterranean. No. September. Lisbon, pp. 26–30.

Cobelli, P. J., Maurel, A., Pagneux, V., Petitjeans, P., 2009. Global measurement of water waves by Fourier transform profilometry. Experiments in Fluids 46 (6), 1037–1047.

Deparday, J., Bot, P., Hauville, F., Motta, D., Le Pelley, D. J., Flay, R. G., 2014. Dynamic measurements of pressures, sail shape and forces on a full-scale spinnaker. In: 23rd HISWA Symposium on Yacht Design and Yacht Construction. Amsterdam.

Durand, M., Leroyer, A., Lothodé, C., Hauville, F., Visonneau, M., Floch, R., Guillaume, L., 2014. FSI investigation on stability of downwind sails with an automatic dynamic trimming. Ocean Engineering 90, 129–139. URL http://linkinghub.elsevier.com/retrieve/pii/S002980181400345X

Eos Systems Inc., 2015. Photomodeler 2015 User Guide.

Fossati, F., 2009. Aero-Hydrodynamics and the Performance of Sailing Yachts: The Science Behind Sailing Yachts and Their Design. International Marine / Mc Graw Hill.

Fossati, F., Bayati, I., Orlandini, F., Muggiasca, S., Vandone, A., Mainetti, G., Sala, R., Bertorello, C., Begovic, E., 2015a. A novel full scale laboratory for yacht engineering research. Ocean Engineering 104, 219–237. URL http://linkinghub.elsevier.com/retrieve/pii/S0029801815001730

Fossati, F., Mainetti, G., Malandra, M., Sala, R., Schito, P., Vandone, A., 2015b. Offwind sail flying shapes detection. In: 5th High Performance Yacht Design Conference. Auckland, pp. 48–59.

Le Pelley, D., Modral, O., 2008. VSPARS: A combined sail and rig recognition system using imaging techniques. In: 3rd High Performance Yacht Design Conference. Vol. 14. Auckland, pp. 57–66.

Lombardi, M., Cremonesi, M., Giampieri, A., Parolini, N., 2012. A strongly coupled fluid-structure interaction model for wind-sail simulation. In: 4th High Performance Yacht Design Conference. Auckland, pp. 212–221.

Masuyama, Y., 2014. The work achieved with the sail dynamometer boat "Fujin", and the role of full scale tests as the bridge between model tests and CFD. Ocean Engineering 90 (November 2014), 72–83.
URL http://linkinghub.elsevier.com/retrieve/pii/S0029801814002509

Mausolf, J., Deparday, J., Graf, K., Renzsch, H., Böhm, C., 2011. Photogrammetry Based Flying Shape Investigation of Downwind Sails in the Wind Tunnel and at Full Scale on a Sailing Yacht. In: 20th Cheasapeake Sailing Yacht Symposium. No. March. Annapolis, pp. 33–43.

Motta, D., Flay, R., Richards, P., Pelley, D. L., Bot, P., Deparday, J., 2015. An investigation of the dynamic behaviour of asymmetric spinnakers at full-scale. In: 5th High Performance Yacht Design Conference. Auckland, pp. 76–85.

Pappa, R. S., Black, J. T., Blandino, J. R., Jones, T. W., Danehy, P. M., Dorrington, A. A., 2003. Dot-Projection Photogrammetry and Videogrammetry of Gossamer Space Structures. Journal of Spacecraft and Rockets 40 (6), 858–867.
URL http://arc.aiaa.org/doi/10.2514/2.7047

Pitcher, N. A., Black, J. T., Reeder, M. F., Maple, R. C., may 2009. Videogrammetry Dynamics Measurements of a Lightweight Flexible Wing in a Wind Tunnel. In: 50th AIAA/ASME/ASCE/AHS/ASC Structures,

Structural Dynamics, and Materials Conference 17th AIAA/ASME/AHS Adaptive Structures Conference 11th AIAA No. American Institute of Aeronautics and Astronautics, Palm Springs, California.
URL http://arc.aiaa.org/doi/abs/10.2514/6.2009-2416

Ranzenbach, R., Armitage, D., Carrau, A., 2013. Mainsail Planform Optimization for IRC 52 Using Fluid Structure Interaction. In: 21st Chesapeake Sailing Yacht Symposium. No. March. Annapolis, pp. 50–58.

Ranzenbach, R., Kleene, J., 2002. Utility of flying shapes in the development of offwind sail design database. In: High Performance Yacht Design Conference. Auckland.

Renzsch, H., Graf, K., 2013. An experimental validation case for fluid-structure-interaction simulations of downwind sails. In: 21st Chesapeake Sailing Yacht Symposium. No. March. Annapolis, pp. 59–66.

Salzmann, M., Fua, P., may 2011. Linear local models for monocular reconstruction of deformable surfaces. IEEE transactions on pattern analysis and machine intelligence 33 (5), 931–44.
URL http://www.ncbi.nlm.nih.gov/pubmed/20733216